Landslides
November 2024, Volume 21, Pages 2695-2709
https://doi.org/10.1007/s10346-024-02317-6 https://archimer.ifremer.fr/doc/00901/101258/

3D stability analysis of submarine slopes: a probabilistic approach incorporating strain-softening behaviour

Sultan Nabil [1, *], Garziglia Sebastien [1]

[1] Geo-Ocean ALMA, UMR6538 - Ifremer, CNRS, UBO, UBS, 29280, Plouzané, France

* Corresponding author : Nabil Sultan, email address : nabil.sultan@ifremer.fr

Abstract :

Submarine landslides exhibiting extreme geometrical and run-out characteristics have been identified and mapped along most continental margins; raising concerns about potential risks to populations should similar events occur. Hazards associated with such events have frequently been assessed using approximations, resulting in data unsuitable for mitigation strategies. Three approximations appear consequential: (i) addressing the problem in two dimensions, thereby neglecting the effect of complex morphology; (ii) employing a deterministic approach that disregards uncertainty related to the heterogeneity of sediment properties; and (iii) treating the sediment as a perfectly elastic–plastic material, simplifying the mechanical behaviour and overlooking the degradation of sediment mechanical properties (strain softening) during different phases of slope movement. Here, we introduced the strain-softening behaviour into a 3D slope stability model. Identification of the critical failure surface was conducted in terms of the probability of failure, considering the influence of sediment parameter variability and uncertainty on the likelihood of failure. The developed model was then used to assess the slope stability of a well-studied example from the literature, the Nice slope (SE France). Our findings indicate that neglecting lateral morphological changes leads to an overestimation of the probability of failure. Additionally, we demonstrated that strain-softening behaviour could significantly affect the factor of safety and the probability of failure for the studied slopes. We argue that a risk assessment and definition of a mitigation strategy require well-advanced characterisation of the mechanical behaviour of sedimentary layers and an analysis incorporating the complex morphology of submarine slopes.

Keywords : 3D slope stability analysis, Limit analysis method, probabilistic analysis, Strain softening

Introduction

Submarine landslides have been identified and mapped along most active and passive continental margins (Harbitz et al. 2014, Urgeles and Camerlenghi 2013, Urlaub et al. 2013) and at different water depths (Masson et al. 2006, Mountjoy and Micallef 2018). Some of these events are associated with landslide tsunamis, which constitute a low-probability but high-risk natural hazard (ten Brink et al. 2014). Some recent submarine landslide events are notable for their devastating impact, such as the 1929 Grand Banks earthquake, which triggered a major submarine slide generating a 20-m tsunami wave (Locat and Lee 2002, Piper et al. 1988) or the 1998 Papua New Guinea tsunami (Tappin et al. 2008) that killed over 2100 people (Synolakis et al. 2002). Several other examples of landslide tsunami have been described in the literature (Harbitz, Løvholt and Bungum 2014, Sassa et al. 2016) and in the absence of sedimentary deposits, these events have been analysed through numerical modelling. This highlights the need to assess the dangers and risks associated with submarine landslides to define appropriate mitigation schemes (Vanneste et al. 2013).

Landslide-tsunami analyses and mainly Probabilistic Tsunami Hazard Assessment (PTHA) applied to large surface areas (basins, seas, oceans) are often based on significant approximations inherent to the lack of information on landslide zones and volume (Geist and Lynett 2014), landslide occurrence frequency and field data (Løvholt et al. 2020). In such an analysis, it is almost impossible to go beyond relying on existing low-resolution bathymetric data and rare-recorded dated events (if any) to define the most critical landslide scenarios and determine the probable maximum flooding probability and the related return period. This raises questions about the efficacy of conducting complex analyses with such considerable uncertainties (Behrens et al. 2021, Geist and Lynett 2014, Zengaffinen-Morris et al. 2022). However, the accuracy of a landslide PTHA study significantly improves when applied to geographically restricted areas with available high-resolution bathymetric and field data (Zengaffinen-Morris, Urgeles and Løvholt 2022).

This paper focuses on characterising the source (geometry, volume, and sediment behaviour), a key element in landslide-tsunami and PTHA analysis (Bullard et al. 2019, Bullard et al. 2023, Satake and Kanamori 1991), by introducing a probabilistic approach that more effectively integrates complex morphologies and the nonlinear behaviour of natural sediments. Strain softening of natural sediments was implemented in a 3D slope stability model (SAMU-3D) (Sultan et al. 2007). This was achieved by adding shear-strain field compatibility consistent with velocity field compatibility (Sultan et al. 2011), to the classical limit analysis method (Chen et al. 2001). Identification of the critical failure surface was conducted in terms of the probability of failure, considering the influence of sediment parameter variability and uncertainty on the likelihood of failure (Lacasse and Nadim 1998). In this analysis the focus was on the continental shelf and upper slope offshore Nice Airport, SE France, especially because of the availability of a set of sediment parameters derived from both laboratory and in situ measurements. This together with the availability of recent, high resolution bathymetry data was instrumental in identifying the key elements affecting not only the geometry of the landslide (source) but also the sensitivity of the calculation results in terms of the probability of failure. Specifically, attention was given to the degradation of the mechanical properties of the sediment (strain softening) during a landslide failure (Lo and Lee 1973, Zhang et al. 2019), the natural variability of the mechanical properties of the sediment (Juang et al. 2019), and the complex morphology of the slope.

Case study conditions – The Nice Slope (SE France)

Geological context, seafloor morphology

Offshore Nice Airport, in SE France, the continental shelf extends typically less than 1.3 km down to 20-30 m water depth. It is bordered to the south by a steep continental slope dipping up to 30° basinwards (Kelner et al. 2016). The continental shelf and upper slope are covered by up to 50 m of pro-delta silty clay sediments containing free and/or dissolved gas (Anthony and Julian 1997, Dan et al. 2007, Garziglia et al. 2021, Kopf et al. 2016, Sultan et al. 2010). Part of this sedimentary unit was removed by a tsunamigenic submarine landslide on October 16, 1979 (Anthony and Julian 1997, Dan, Sultan and Savoye 2007). This event produced slopes which locally attain maximum angles of 48° in the sidewalls of the scar (Kelner, Migeon, Tric, Couboulex, Dano, Lebourg and Taboada 2016). Leynaud and Sultan (2010) carried out a probabilistic 3D slope stability analysis of one of the steepest areas with the SAMU-3D software by accounting for the variability and uncertainty in sediment strength as derived from piezocone soundings over the continental shelf. While some strength profiles near the border of the shelf indicated the presence of local shear zones from about 19 m to 28 m below seafloor, the authors assumed that the associated strength degradation was widespread over a continuous weak layer in their model (Leynaud and Sultan 2010). As a result of the analysis, they estimated that the ovoid-shaped area outlined in red in Fig. 1 has a maximum probability of 50% to fail in undrained conditions.

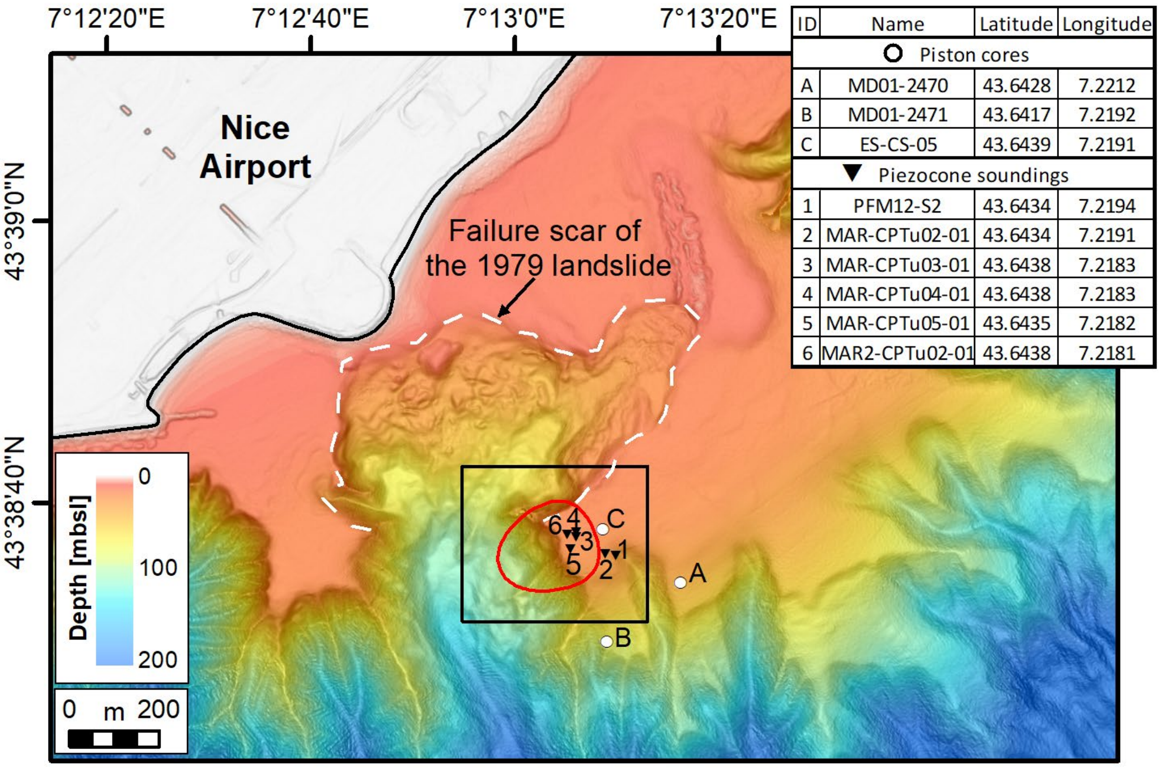

ID	Name	Latitude	Longitude
	Piston cores		
A	MD01-2470	43.6428	7.2212
B	MD01-2471	43.6417	7.2192
C	ES-CS-05	43.6439	7.2191
	Piezocone soundings		
1	PFM12-S2	43.6434	7.2194
2	MAR-CPTu02-01	43.6434	7.2191
3	MAR-CPTu03-01	43.6438	7.2183
4	MAR-CPTu04-01	43.6438	7.2183
5	MAR-CPTu05-01	43.6435	7.2182
6	MAR2-CPTu02-01	43.6438	7.2181

Fig. 1 Shaded bathymetry map of the continental shelf and upper slope offshore Nice Airport. As indicated in the inset legend, white circles and black triangles correspond to coring and piezocone sounding sites, respectively (data in Fig. 2). The red ovoid-shaped feature is the contour of the most critical failure surface according to Leynaud and Sultan (2010). The black rectangle indicates the area shown in Fig. 3

Geotechnical properties and shear zone development

This study relies on submerged unit weight, *γ'*, and undrained shear strength, *Su*, data from three piston cores and six piezocone soundings obtained within or in the immediate vicinity of the area where Leynaud and Sultan (2010) estimated a probability of failure of 50% (Fig. 1).

Piston core data

Data obtained on piston cores MD01-2470, MD01-2471 and ES-CS05 were previously presented in Sultan et al. (2004) and Garziglia et al. (2021). To estimate representative profiles of *γ*' and *Su* along with the associated natural variability of these parameters, attention was given to avoid data that might have been affected by gas exsolution upon core recovery. Hence, the depth of the seismically imaged gas front reported in Sultan et al. (2010) and Garziglia et al., (2021) was used to discard data below 4.65 m in core ES-CS05 and below 6.25 m in cores MD01-2470 and MD01-2471.

Gamma density profiles obtained by logging cores with a spacing of 1 cm were converted into the submerged unit weight profiles shown in Fig. 2a by considering a seawater unit weight of 10.1 kN/m^3. Analysis of the upper part of the three cores reveals that the curve that best fits the data is of the following form: $\gamma' = 6.95 + z^{0.38}$ with a standard deviation $SD_{\gamma'}$ of 0.75 kN/m^3. The data obtained with this equation down to 50 m below seafloor were used as mean gamma density values in the subsequent slope stability analyses.

Undrained shear strength was measured with a motorised vane shear at a spacing of 15 cm on the three cores (Fig. 2c). Using standard linear regression, the line to best fit the data is $Su = 0.88z + 3.7$ and the standard deviation is SD_{Su}=3.1 kPa.

Piezocone sounding data

In addition to the data from sounding PFM12-S2 previously reported by Sultan et al. (2010) and Leynaud and Sultan (2010), those from five new piezocone soundings carried out during the Marolis PENFELD and Marolis 2021 cruises are considered in the present study. The new soundings were performed with the Penfeld seabed rig which pushed a 10 cm^2, pressure compensated piezocone at a standard rate of 2 cm/s down to 50 m below seafloor. A differential pressure sensor at the cone shoulder position measured penetration pore pressures relative to hydrostatic (Δu_2) which were then used to derive corrected tip resistance (q_t) according to ISO 22476-1. A study area specific gradient Δu_2=14.7z was derived from the best linear fit to the data obtained during undrained penetration, that is within the mostly clayey sediments encountered down to 50 m below seafloor. This gradient was used to refine the q_t profile from sounding PFM12-S2 reported by Leynaud & Sultan (2010) as it suffered a lack of precise penetration pore-pressure measurements. Undrained shear strength values were then derived from filtered q_t profiles using the following formula (Lunne et al. 2002):

$$Su = \frac{q_t - \sigma_{v0}}{N_{kt}} \quad (1)$$

where the total in-situ vertical stress, σ_{v0}, was determined from the curve which best fits the unit weight data derived from gamma-density logging of the upper 4.65 m in core ES-CS05 and upper 6.25 m in cores MD01-2470 and MD01-2471; that is $\gamma = 17.03 + z^{0.38}$. Based on correlations with *Su* values obtained from motorised vane shear tests on cores, the cone factor N_{kt} was taken to be equal to 25.

Fig. 2b illustrates that below approximately 20 m depth the trend of PFM12-S2 and MAR2-CPTu02-01 q_t profiles departs from that of the four other soundings as evidence of strength weakening associated with shear zones previously reported by Sultan et al. (2010). Accordingly, PFM12-S2 and MAR2-CPTu02-01 data were discarded from the linear regression analysis aiming at estimating a representative undrained shear strength (Su) gradient with depth along with the associated natural variability. This analysis revealed that the line to best fit the data from the four soundings shown in yellow in Fig. 2 is $Su = 0.89z + 8.6$ and the standard deviation is SD_{Su}=3.1 kPa (Fig. 2c). The data obtained with this equation down to 50 m below seafloor were used as mean Su values in the subsequent slope stability analyses. As previously suspected from q_t profiles, below approximately 20 m depth, *Su* data derived from PFM12-S02 and MAR2-CPTu02-01 soundings plot below this trend (Fig. 2). In line with Sultan et al. (2010) who ascribed this to the occurrence of shear zones, here, it is taken to provide a measure of post-peak strength degradation in the field. Accordingly, as shown in Fig. 2c, sediment strength sensitivity, *St*, is estimated to range from 1.45 to 1.71 with a mean value of 1.55. This sensitivity value was considered as constant over the upper 50 m of sediment in the subsequent slope stability analyses.

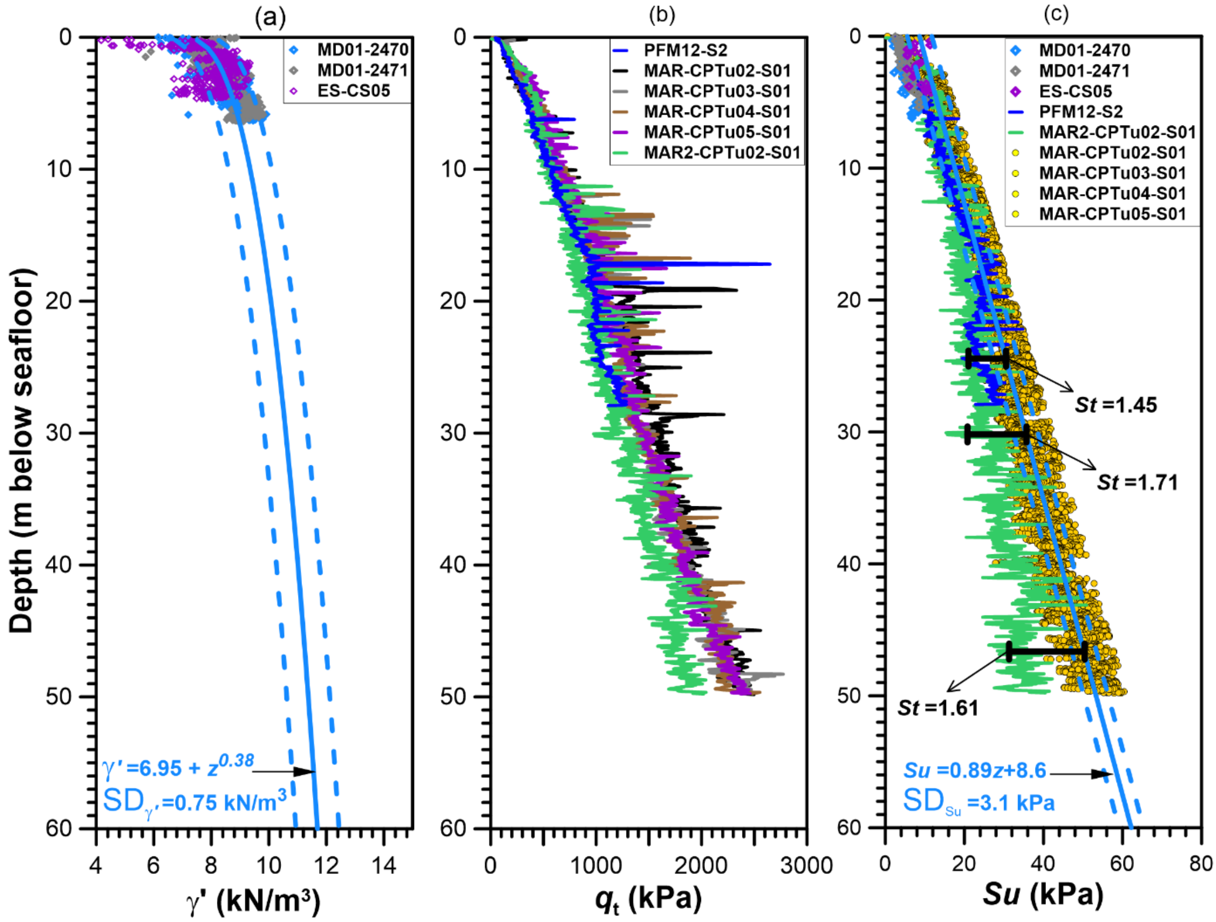

Fig. 2 **a** Depth profiles of submerged unit weight (γ') from three piston cores located in Fig. 1. The equation of the curve of best fit (solid blue) to data is indicated together with the standard deviation, SD (dashed blue curves). **b** Depth profiles of corrected cone resistance, q_t, from six piezocone soundings (see Fig. 1 for location). **c** Undrained shear strength, *Su*, measured on three piston cores and derived from six piezocone soundings. The solid blue line is the linear regression fitted to the data shown in yellow while the dashed blue lines correspond to ± 1 standard deviation (*SD*). Strength sensitivity (S_t) is estimated to be the ratio between *Su* from the best-fit line to that derived from soundings PFM12-S2 and MAR2—CPTu02-S01

3D Site stratigraphy

3D site stratigraphy is a crucial input for accurate analysis of the 3D slope stability of the study zone. The data presented in Fig. 2 reveal a predominantly uniform lithology, with the exception of some fine layers of coarse sediments (mainly silty sand). The intact sediment on the plateau exhibits an almost linear variation with depth in *Su* and a continuous change in γ'. However, substantial erosion and slope instabilities have significantly shaped the study area, resulting in the presence of over-consolidated sediments (maximum past effective vertical stress exceeds the present effective overburden stress) that outcrop at the seabed. The only region unaffected by gravitational events and erosion is located in the southeast of the study area (surrounding profile 2 in Fig. 3).

We reconstructed a hypothetical bathymetry prior to the occurrence of landslides and erosion using an average slope matching that of the unaffected zone to the southeast (contour lines in Fig. 3a). We considered the presence of eight sedimentary layers parallel to the pre-landslide morphology within the first 50 metres beneath the seabed which provided accurate discretisation of the *Su* and γ' profiles (Table 1). The present 3D stratigraphy was derived by eroding the restored bathymetry to fit with that of the present-day. The cross sections shown in Fig. 3b illustrate the complex impact of landslides and erosion on the 3D geometry of the sedimentary layers, notably in some areas where sediment from deep layers outcrops at the seabed, stressing the need to account for the over-consolidation state of the sediment in calculations. However, it is crucial to note that landslides, erosion, and sediment depositions frequently occur simultaneously, so the approach used to define the present 3D stratigraphy may oversimplify the sedimentary architecture of a natural environment.

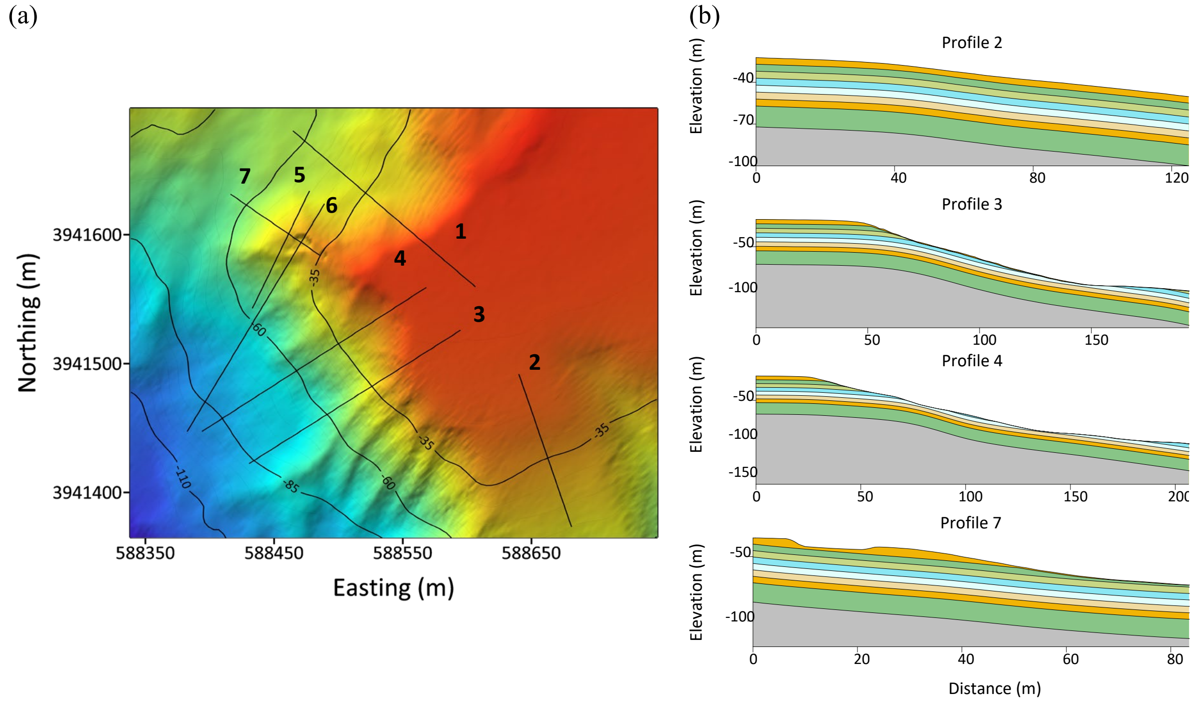

Fig. 3 **a** Shaded bathymetry of the study zone with contour lines representing the reconstructed bathymetry obtained through a homogeneous extension of the intact sedimentary body located to the southeast of the map. Positions of the 7 cross sections are also projected on the map. **b** Cross sections 2, 3, 4, and 7 illustrate the geometry of 8 sedimentary layers affected by previous erosion and submarine landslides shaping the area.

Layer	Thickness	Depth below seafloor	*Su*			*γ'*		
			μ_{Su}	SD_{Su}	COV_{Su}	$\mu_{\gamma'}$	$SD_{\gamma'}$	$COV_{\gamma'}$
	(m)	(m)	(kPa)			(kN/m^3)		
1	5	5	11	3.1	0.28	8.79	0.75	0.09
2	5	10	15	3.1	0.21	9.35	0.75	0.08
3	5	15	20	3.1	0.16	9.75	0.75	0.08
4	5	20	24	3.1	0.13	10.07	0.75	0.07
5	5	25	29	3.1	0.11	10.35	0.75	0.07
6	5	30	33	3.1	0.09	10.59	0.75	0.07
7	5	35	38	3.1	0.08	11.81	0.75	0.06
8	15	50	46	3.1	**0.07**	11.37	0.75	**0.07**

Table 1 Geotechnical properties including the undrained shear strength *Su* and the submerged unit weight *γ'* for the considered 8 layers. For *Su* and *γ'*, a mean value *μ*, a standard deviation SD and a coefficient of variation COV are given

Slope stability analysis – methods

2D slope stability analysis (OPTUM G2)

A 2D Finite Element Analysis (FEM) was conducted using the Optum G2 software (Krabbenhoft et al. 2015) wherein the sediment was assumed to obey Tresca's failure criterion for clay. Optum G2 is a finite element program for strength and deformation analysis under plane strain conditions.

3D slope stability analysis

Limit equilibrium method: Scoops3D

Scoops3D, developed by the U.S. Geological Survey, allows to evaluate three-dimensional slope stability of complex digital elevation models (DEM) (Reid et al. 2015). The programme uses a three-dimensional (3D) method of column limit-equilibrium analysis to evaluate the stability of millions of potential landslides. Scoops3D assesses the stability of a spherical slip surface involving numerous Digital Elevation Model (DEM) cells. The software identifies the least stable potential landslide for each DEM cell by calculating its Factor of Safety (FoS) and determining the associated failure volumes. The software uses the ordinary (Fellenius 1936) or Bishop's simplified method (Bishop 1955), which both neglect side forces between the columns in a potential failure mass. The sediment is considered to behave as a simple linear Coulomb-Terzaghi material (cohesion and the internal friction angle characterise the sediment). It is possible to incorporate into the calculation the effect of excess pore pressure generated by external factors such as rainfall (Tran et al. 2018), or to perform a simple analysis under undrained conditions, exclusively requiring the introduction of undrained cohesion (shear strength) and density values.

Limit analysis method: SAMU-3D

SAMU-3D (Sultan, Gaudin, Berne, Canals, Urgeles and Lafuerza 2007) is a 3D slope stability analysis model based on the limit analysis method and the upper bound theorem of plasticity (Chen, Wang, Haberfield, Yin and Wang 2001, Michalowski 1995). SAMU-3D requires postulating a valid failure surface that satisfies the mechanical boundary conditions and a velocity field that satisfies the boundary conditions in the sediment delimited by the failure surface. In SAMU-3D, the postulated failure surface is not spherical and depends on eight shape parameters in order to identify as accurately as possible the most critical failure surface. Two shape parameters define the ellipticity of the failure surface in both the horizontal and vertical planes. Within the horizontal plane, four parameters govern both the size and shape of the failure surface, while an additional two shape parameters specify its curvature within the same plane. The graphical representation of these shape parameters is shown in (Sultan et al., 2007). The 3D approach proposed in SAMU-3D approximates the failure surface by discretising the sediment mass bounded by the postulated rupture surface into a number of prisms. For the velocity field, the sediment is considered as a Mohr–Coulomb material with an associative flow rule (Chen, Wang, Haberfield, Yin and Wang 2001, Michalowski 1995). The sediment will collapse if the work generated by the external loads through any mechanism of collapse exceeds the internal plastic dissipation. Under these conditions, the upper bound theorem states that all possible external loads applied to a kinematically admissible plastic zone, minimising the work-energy balance equation (Rate of internal energy dissipation = Rate of external work) can approach the external load that results in failure. With the proposed method, the traditional definition of FoS is conserved so that the results from the proposed model can be directly compared with other slope stability analysis methods. For a given load generated by external mechanisms, the 3D critical failure surface corresponding to the minimum FoS, is identified by means of optimisation with respect to the different shape parameters. Indeed, evaluation of the stability of a slope becomes a numerical problem of finding a set of variables that provides the minimum FoS. Validation of SAMU-3D is detailed in Sultan and co-authors' work (Sultan, Gaudin, Berne, Canals, Urgeles and Lafuerza 2007), which used literature data comparisons. The study primarily relied on examples considered by Hungr and co-authors (Hungr et al. 1989).

Probabilistic analysis

A Fortran script was developed to generate two independent uniform random numbers using Fortran's RANDOM_SEED and RANDOM_NUMBER functions. The Box-Muller transform (Box and Muller 1958) was then applied, converting these uniform variables into pairs of independent standard normal variables. Subsequently, the generated standard normal variables were scaled and shifted to produce random numbers conforming to a normal distribution with user-defined mean and standard deviation. Following (Hicks and Samy 2002) a normal distribution was considered convenient given the low to intermediate values of coefficient of variation (e.g. 0.1-0.3) reported in Table 1. The script was used to write a large number (~ 1000) of input files for each run using Scoops3D and SAMU-3D. Fig. 4 illustrates the normal distribution of the undrained shear strength and submerged unit weight values for layers one and two as used in a set of 1000 input files. All the following analyses were conducted under undrained conditions since the paper focuses on studying the approximations used in the case of a sudden, catastrophic landslide affecting the water column and potentially the generation of a tsunami (landslide-tsunami).

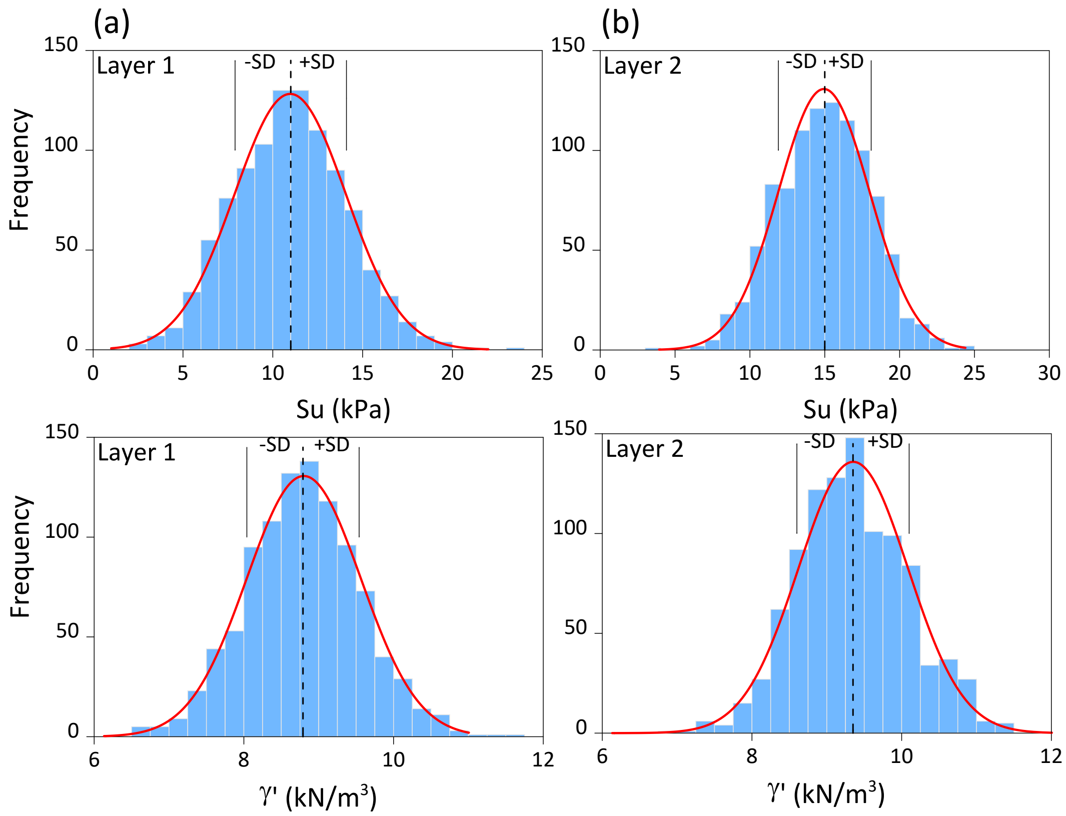

Fig. 4 Normal distribution of used *Su* and *γ′* values for **a** layer 1 and **b** layer 2 in Scoops3D and SAMU-3D runs

In this particular approach, addressing the dependence of random variables becomes crucial. To achieve this, we examined the distribution of both *Su* and *γ′* variables across all layers and calculations under consideration. As illustrated in Fig. 5, the distribution exhibited a distinct randomness, attesting that the values of *Su* and *γ′* are intrinsically independent.

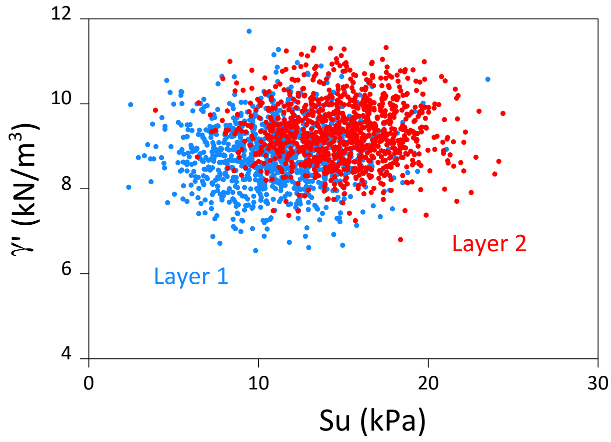

Fig. 5 Distribution of *Su* and *γ′* in layers 1 and 2 for a set of 1000 input files

The probabilistic parallel calculations were conducted using DATARMOR (https://www.ifremer.fr/fr/infrastructures-de-recherche/le-supercalculateur-datarmor), a high-performance computing (HPC) resource, and data-storage infrastructure. The resulting output files were analysed in terms of minimum, maximum, and mean values of FoS and the associated failure volumes. The probability of failure was subsequently determined for each set of calculations.

Introduction of strain-softening behaviour to SAMU-3D

To accurately account for the strain-softening behaviour of a natural sediment in SAMU-3D, it was crucial to use a versatile curve capable of describing the three main phases of a stress/strain curve. This curve incorporates the elastic behaviour, mobilization of the peak shear value (τ_p) and the softening behaviour as the shear strain increases (Fig. 6). In the present work, we used the expression proposed by Sultan and co-authors (Sultan, Garziglia and Colliat 2011) giving the shear strength τ normalised with respect to the peak shear strength τ_p as a function of shear strain δ (Eq. 2).

$$\frac{\tau}{\tau_p} = \left(1 - e^{-\beta\delta}\right) + \left(e^{-\omega\delta^{\alpha}} - 1\right)\left(1 - \frac{1}{S_t}\right) \qquad (2)$$

In equation 2, β corresponds to the elastic stiffness of the material and is proportional to Young's modulus; S_t is the sensitivity and α and ω are two shape parameters used to describe the decrease in shear strength from the peak to residual value (Fig. 6).

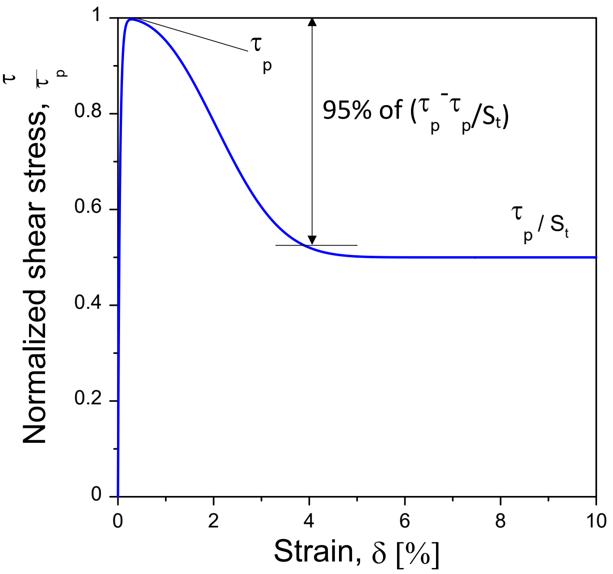

Fig. 6 Normalised shear stress - strain curve used to implement strain-softening behaviour in SAMU-3D

To include the strain-softening behaviour in SAMU-3D software, a shear strain field compatibility equivalent to the velocity field compatibility (Chen, Wang, Haberfield, Yin and Wang 2001) used in the limit analysis method was considered. Zhang and co-author (Zhang and Zhang 2007) have already used a similar development combining a compatible shear strain field to a 2D limit equilibrium method. The calculation is done by introducing an additional numerical loop, where at each step, the shear strain field was determined for the whole postulated failure volume by increasing incrementally the applied shear strain δ applied at the bottom of the first slice. Using the stress/strain curve equivalent to that presented in Fig. 6, it is possible to calculate the mobilised shear strengths at the bottom of prisms and between adjacent prisms. For each shear strain δ applied at the bottom of the first slice a FoS value was calculated (Fig. 7). Zhang and Zhang (2007), considered that the true shear strain δ should be the one that leads to the maximum FoS among all the possible values (Fig. 7a). However, by using this criterion, the minimum shear strength mobilised between different adjacent prisms and at the bottom of the failure surface rarely reaches the remolded shear strength. On the other hand, recent publications (Dey et al. 2015, Dey et al. 2016, Islam et al. 2019) examining the impact of strain softening on slope stability and employing advanced finite element calculations demonstrate that slope failures are initiated when the mobilised shear strength is reduced by 95% from peak at certain locations along the failure surface. In this work, we propose to consider the true shear strain δ corresponding to the critical FoS as the one leading to the reduction of the undrained shear strength by 95% of (τ_p - τ_p/S_t) at least at one location along the failure surface (Fig. 7a, b). Fig. 7c illustrates how the normalised shear strength can reach critical values at the lower edge of the basal failure surface (dashed red area), while the majority of interslice normalised shear strengths remain in the elastic domain (blue dots in Fig. 7b).

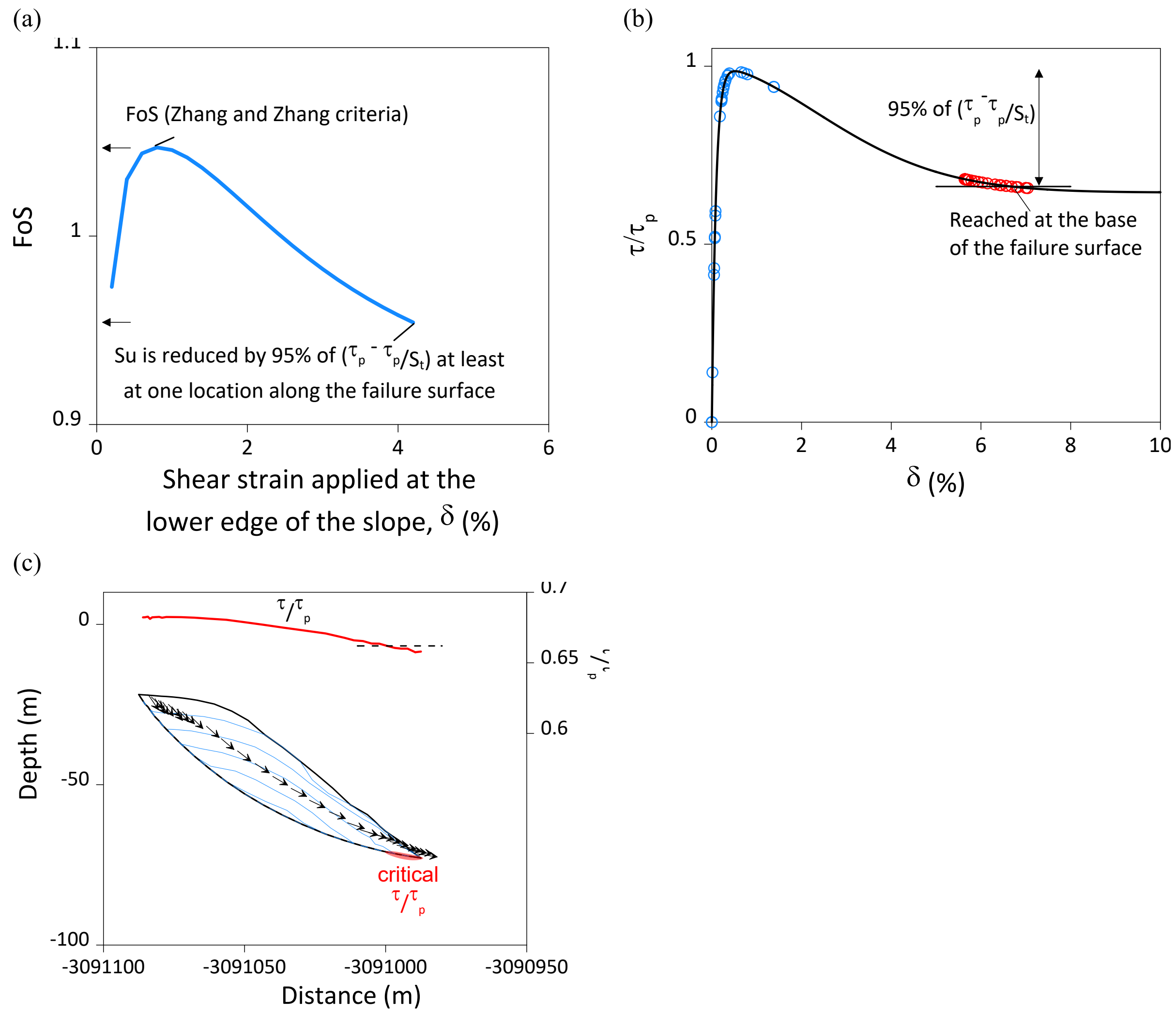

Fig. 7 a Criteria used to define the critical FoS for strain softening materials. **b** Normalised shear strengths mobilised for the critical FoS at the bottom of the failure surface (red dots) and between adjacent prisms (blue dots). **c** 2D cross section along the central axis named in the following the neutral line (NL) of the failure surface, showing the sedimentary layers impacted by the landslide. Most critical zones at the base of the surface in terms of sediment degradation are highlighted by red dashed area. The τ/τ_p along the base of the failure surface is also shown in the figure. The distance in **c** is expressed within a local reference frame aligned with the NL

To the authors' knowledge, no published studies have previously evaluated the 3D slope stability of strain softening, purely cohesive materials. Therefore, the strain-softening module was validated by analysing the mechanism of progressive failure of a 300-m-long 2D slope dipping at 4.2° and consisting of a 20-m-thick layer of marine sensitive clays (S_t=1.53) deposited on top of firmer non-sensitive clay (Andresen and Jostad 2007). The authors used the Plaxis software with the advanced model NGI-ANISOFT in order to evaluate the effect of sensitivity on the shape of the failure surface and to evaluate the load-bearing capacity of an inclined slope. The shape and size of the two failure surfaces predicted by SAMU-3D were comparable to those predicted by Andresen and Jostad (2007) (Sultan, Garziglia and Colliat 2011). The normalised failure load predicted by SAMU-3D was 17% higher than the value reported by Andresen and Jostad (2007) using the NGI-ANISOFT advanced soil model. This result is consistent with findings already demonstrated in the literature, namely that a 2D approach, such as the one used by Andresen and Jostad (2007), underestimates the stability of a slope compared to a 3D approach (Duncan 1996). Additional validation examples are presented in Sultan et al. (2011).

Numerical results, analysis and limitations

2D analysis

A 2D FEM study was conducted using the Optum G2 software (Krabbenhoft, Lyamin and Krabbenhoft 2015) wherein the sediment was assumed to obey Tresca's failure criterion for clay. The considered profile (N° 3) was characterised by the highest mean slope angle of the seven profiles shown in Fig. 3. Each of the eight different layers shown in Fig. 8 is characterised by an undrained shear strength (*Su*) and a submerged unit weight (*γ'*) as reported in Table 1. The FoS calculated using the strength reduction method (SRM) is near zero thus revealing that a 2D calculation is not suited to a complex morphology equivalent to the upper slope offshore Nice. Indeed, along profile three, the slope angle reaches locally a value of 49° which is not representative of the 3D slope. The displacement field shown in Fig. 8 indicates that a displacement discontinuity occurs at the interface between layers seven and eight corresponding to a maximum depth of 35 mbsf.

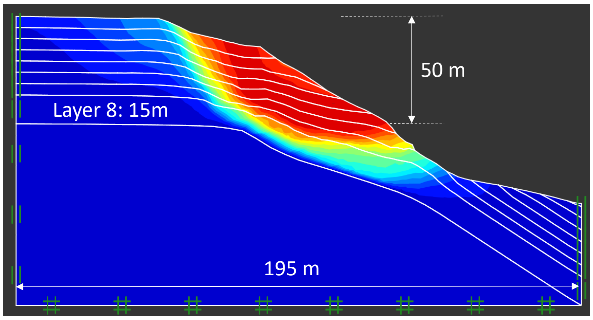

Fig. 8 2D modelled sediment layers and the displacement field projected on the deformed slope using Optum G2. In the strength reduction method, displacement is represented on a relative scale. Colours become warmer as displacement increases (red for high displacement, dark blue for zero displacement).

Probabilistic approach

Scoops3D

The Scoop3D software was used by following the probabilistic approach described in the "Method". We performed 1000 calculations using the DATARMOR supercomputer. The average values of FoS and failure depth are presented in Fig. 9a and b. It is noteworthy that the majority of the analysed area exhibits a FoS below one, indicating the likelihood of deformation and instability processes in this zone. The maximum failure depth was found equal to 32 m mainly at the edge of the plateau (Fig. 9b). Determination of the probability of failure (at each node the number of FoS ≤ 1 divided by 1000) was defined based on the results of the 1000 runs (Fig. 9c). The majority of the analysed area is characterised by a failure probability exceeding 90%.

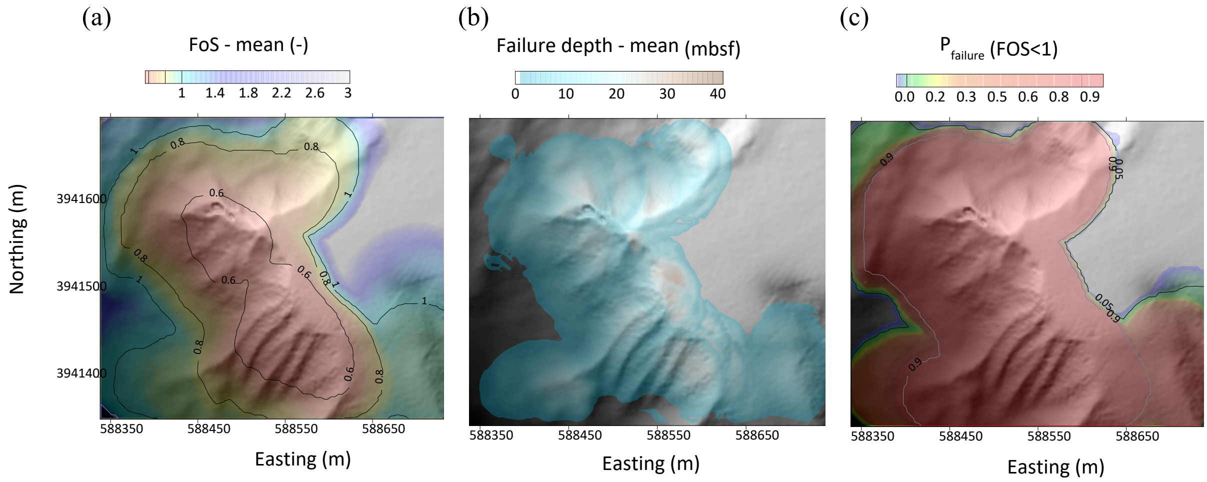

Fig. 9 Mean values of **a** FoS and **b** failure depth obtained from 1000 Scoops3D runs. **c** Probability of failure obtained from 1000 calculations

This result is consistent with the different gravitational events shaping the slope but also with the presence of a shear zone detected through CPTu measurements (Fig. **2**). However, a FoS ≤ 1 does not necessarily imply an immediate catastrophic landslide; it can simply indicate ongoing local deformations and the formation of shear zones (Demers et al. 1999, Mahmoud et al. 2000). The limit equilibrium method used in Scoops3D relies on approximations which means that these results and numbers should be treated with caution. Among these approximations, the following points were listed by Reid and co-authors (Reid, Christian, Brien and Henderson 2015):

- Potential failure surfaces are limited to a spherical representation undergoing rotational slip.
- Ordinary (Fellenius) or Bishop's simplified methods neglect side forces between the columns in a potential failure mass.
- No option for incorporation of sediments with complex, non-linear mechanical behaviour.

In addition to limitations inherent to the limit equilibrium method, in Scoops3D, each spherical surface is analysed independently of the overall morphology as well as of potential adjacent failures, and the final result is a superposition of individual results (Fig. 9). However, this kind of method is relatively easy to implement numerically, and the calculations are sufficiently fast, providing rapid identification of the most critical areas in terms of instability. Consequently, a preliminary assessment thereby contributes to target critical areas for more precise calculations using more suitable methods.

SAMU-3D

Through this approach, an initial deterministic calculation defined the orientation and principal axis (hereafter referred to as the neutral line - NL) characterising the most critical failure surfaces. This choice was made to optimise computation time. Alternatively, with a probabilistic approach involving uncertainty regarding the NL, uncertainty regarding the shape of the failure surface with its eight shape parameters, and uncertainties regarding mechanical properties, we would need to perform a prodigious number of calculations (approximately 2.10^{11}), which even with the DATARMOR supercomputer would not be achievable in reasonable time (> 500 hours). The workflow we adopted is summarised in Fig. 10.

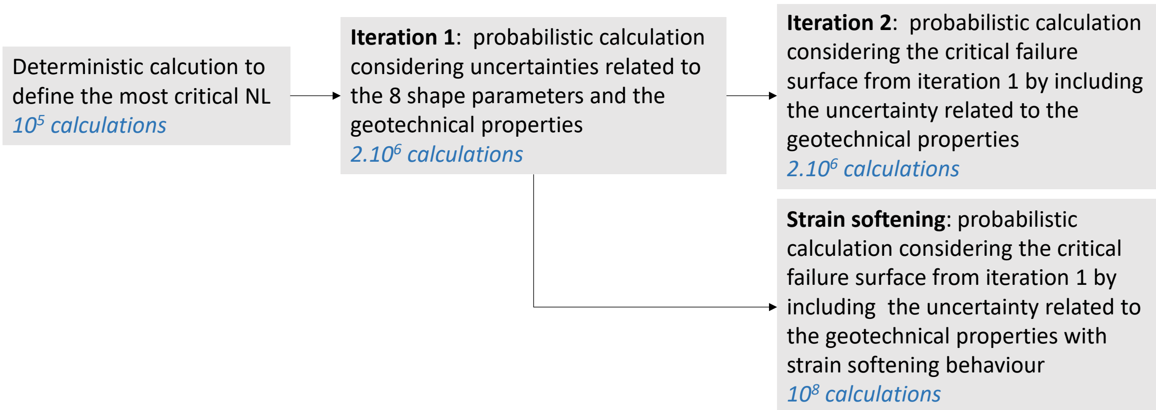

Fig. 10 Workflow calculation

We conducted an initial series of 100,000 deterministic calculations using the mean values of *Su* and γ' (Table 1) associated with the 3D stratigraphy shown in Fig. 3. The minimum FoS was found equal to 1.02 and was reached after 56,091 iterations. The main goal of these preliminary calculations was to identify the most critical Neutral Line (NL) associated with the failure surface with the lowest FoS (NL is shown in Fig. 11).

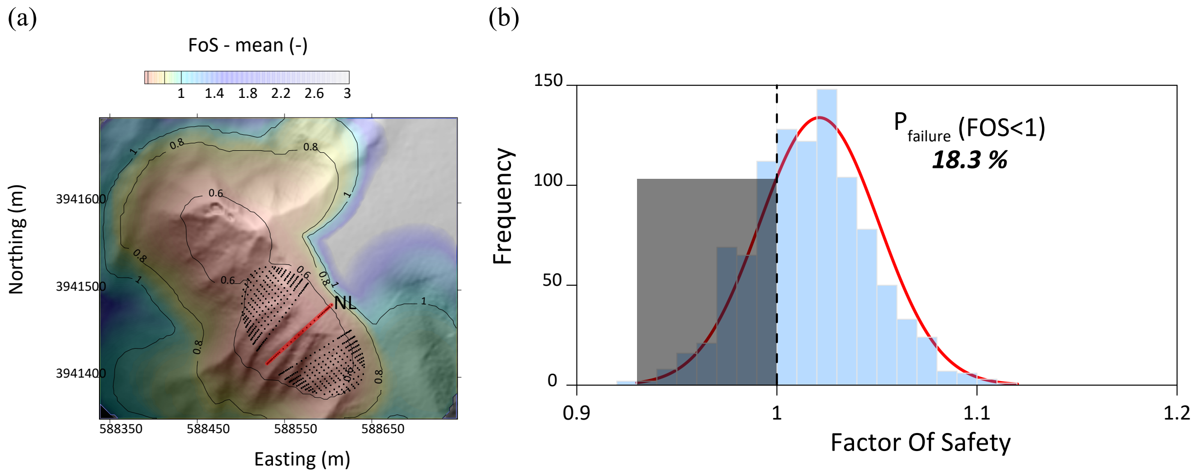

Fig. 11 Iteration 1: **a** Failure surface predicted during iteration 1 with SAMU-3D projected on the mean FoS map obtained by Scoops3D, and **b** Frequency distribution of FoS values for 1000 runs, revealing a probability of failure of 18.3%, significantly below the 90% probability obtained with Scoops3D (see also Fig. 9c)

The first iteration using the probabilistic approach involved the NL obtained with the deterministic approach and allowed the eight shape parameters to vary in order to determine the most critical failure surface obtained from 1000 runs with a probabilistically chosen set of *Su* and γ' data (Table 1). The failure surface shape was optimised by conducting 2000 calculations per run. The total number of calculations for iteration one was 2,000,000, yielding to 1,000 final failure surfaces and their associated FoS. Fig. 11a shows the failure surface with the minimum FoS projected on the FoS-mean values obtained with Scoops3D. The thousand output results enabled us to draw the FoS distribution for this first iteration and determine a failure probability of 18.3% (Fig. 11b). The probability of failure is calculated as the ratio of cases where FoS is < 1 to the total of 1,000 runs. The 3D geometry corresponding to the minimum and maximum FoS, as well as the 2D cross sections along the NL, are shown in Fig. 12 and Fig. 13. Note that the failure surface corresponding to the maximum FoS is deeper than that with the minimum FoS. The maximum failure depth is coherent with the results obtained using Scoops3D (Fig. 9b) and the observed shear zone detected thanks to in-situ CPTu data (Fig. 2).

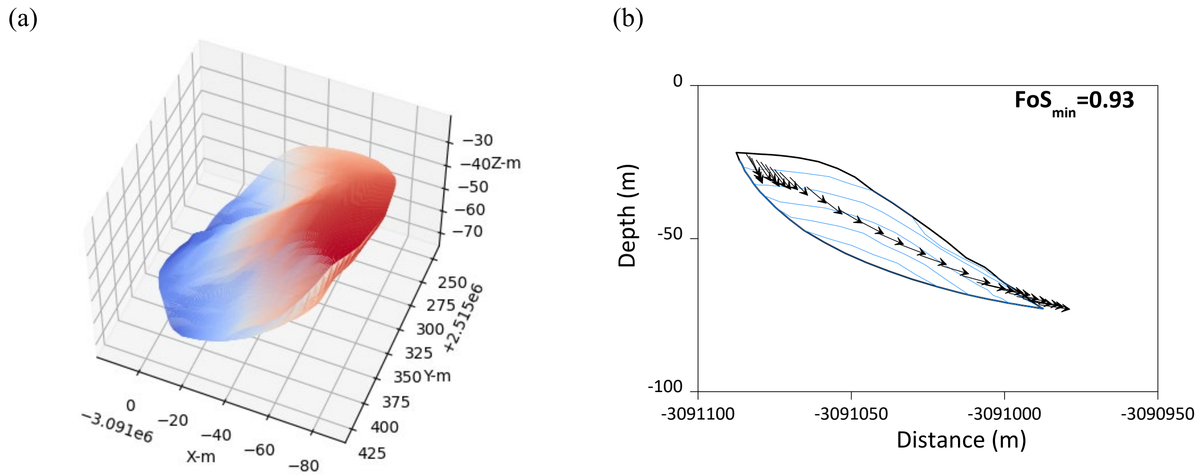

Fig. 12 Iteration 1 - minimum FoS: **a** 3D failure surface, and **b** 2D cross section along the NL revealing the shape of the failure surface and sedimentary layers affected by the slide.

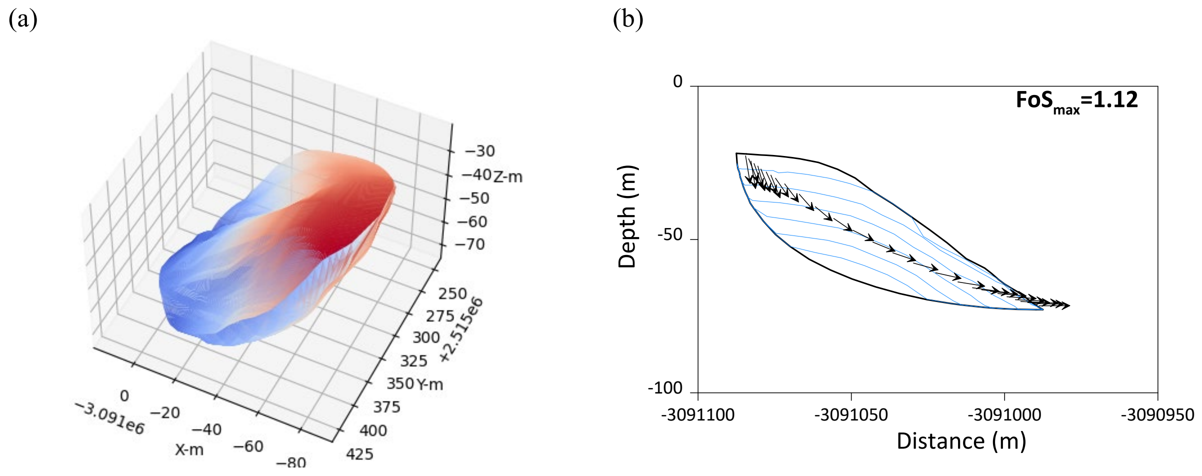

Fig. 13 Iteration 1 - maximum FoS: **a** 3D failure surface, and **b** 2D cross section along the NL revealing the shape of the failure surface and sedimentary layers affected by the slide

Shaded bathymetric maps illustrating predicted post-failure morphologies for both the minimum and maximum FoS values are shown in Fig. 14. The failure volume corresponding to the minimum FoS is 164,937 m^3, whereas the mobilised volume for the maximum FoS is 205,762 m^3.

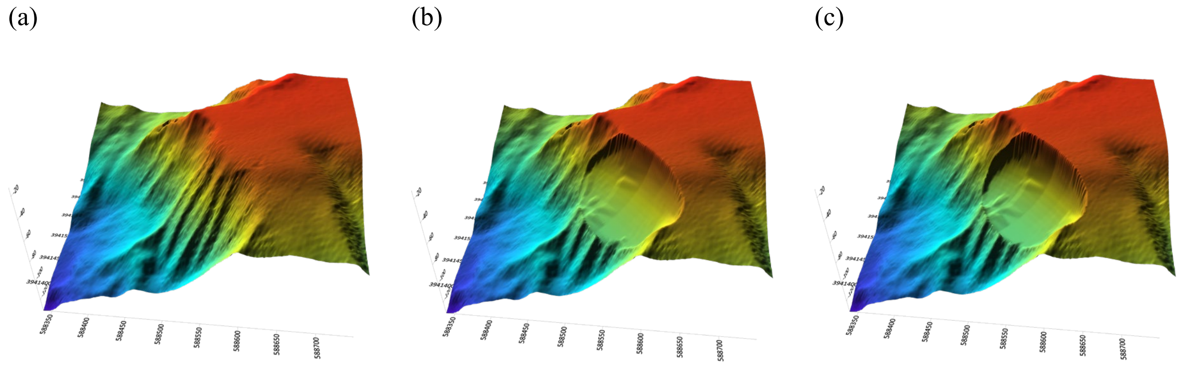

Fig. 14 3D bathymetry of the area analysed using SAMU-3D and the new bathymetry obtained by removing the failure volume for **b** the minimum and **c** the maximum FoS

In iteration two, we fixed the shape parameters corresponding to the most critical failure surface obtained during iteration one (geometry of Fig. 12) and we used a probabilistic distribution of the geotechnical parameters characterising the sedimentary layers in Fig. 3. A total of 1,000 runs were performed, allowing us to slightly improve the calculation results in terms of probability of failure. We obtained a slightly higher probability of failure compared to the previous case, namely 19.9% (Fig. 15).

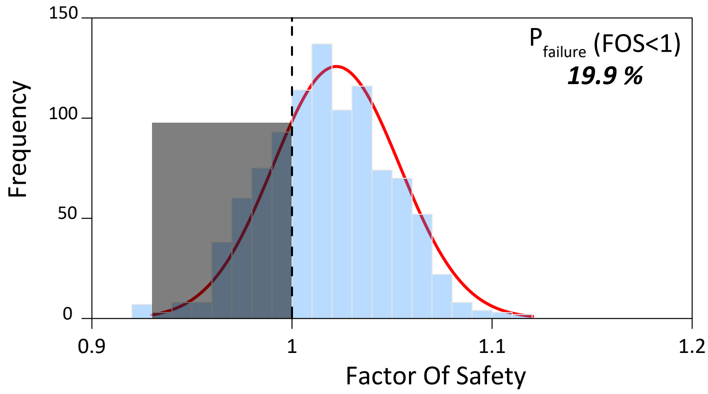

Fig. 15 Distribution of FoS values for 1000 runs, revealing a probability of failure of 19.9 %, slightly higher than iteration 1 but still significantly below the 90% Scoops3D values (see also Fig. 9c)

Strain softening

The geotechnical data obtained on piston cores and derived from piezocone soundings served as input parameters for a conventional slope stability analysis under undrained conditions. Additionally, the detection of shear zones in the field served to estimate sediment sensitivity (Fig. 2c) as a key parameter to account for strain softening through an empirical formulation (Eq. 2). However, site-specific stress-strain curves are insufficient to accurately capture the strain levels at which both peak and residual strengths are reached. Therefore, in the following calculation we consider that residual strength is reached from a shear strain of 10% as suggested by (Skempton 1964) This is long after the shear strain at peak strength which was arbitrarily set to 0.5% based on the triaxial results reported by Lunne and Long (2006) (Lunne and Long 2006) on high quality marine clayey sediment samples. As a consequence, the three parameters of equation two are set equal to the following: $\beta = 11$, $\alpha = 1.8$, $\omega = 0.1$. The sensitivity, S_t, is assumed to be constant and set to 1.55 (Fig. 2c). While these two approximations of shear-strain levels at peak and residual strengths may influence the final calculation results, it is important to note that the primary focus of the paper is on developing approaches rather than conducting an in-depth analysis of a specific case study. Therefore, we consider this approximation acceptable and believe it has no substantial impact on the final conclusion of the paper.

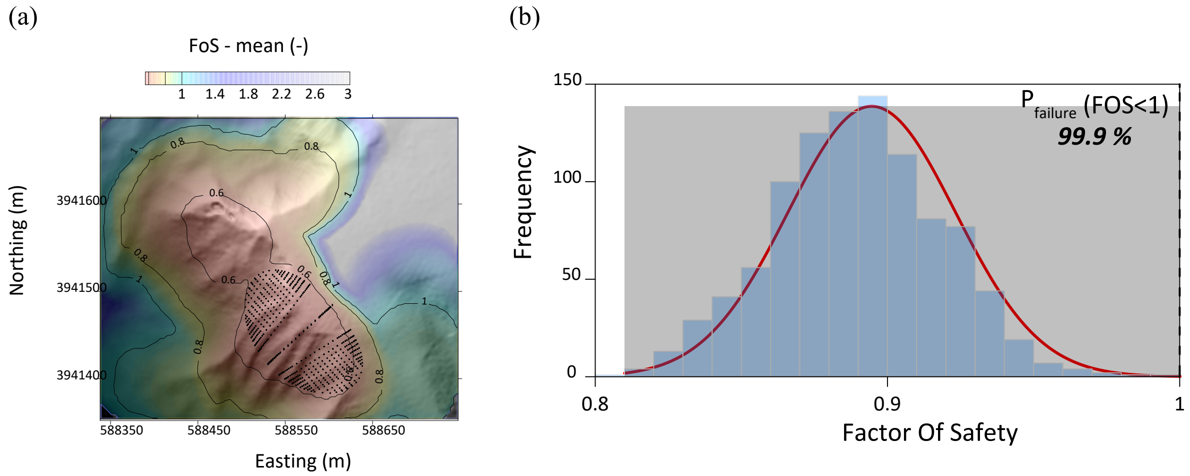

Fig. 16 Calculation with strain-softening behaviour: **a** Failure surface predicted with SAMU-3D projected on the mean FoS map obtained by Scoops3D, and **b** distribution of FoS values for 1000 runs, revealing a 99.9% probability of failure, significantly higher than calculations neglecting the strain-softening behaviour

For the present calculation considering the effect of strain softening, we once again considered the critical NL from Fig. 11a and conducted 1000 runs while optimising shape parameters in each run through 2000 steps. In the case of the strain-softening model, a shear-strain field compatibility is introduced. The stress-strain curve was discretised into 50 increments. At each value of the strain increment, the FoS was calculated, and the final FoS was determined according to the criteria described in Fig. 7a. Therefore, a total of 10^8 (= 1000*2000*50) calculations were performed to obtain 1000 failure surfaces with corresponding failure volumes. The most critical rupture surface (FoS=0.81) was projected on the mean FoS map from Scoops3D in Fig. 14a. The distribution of FoS values for the 1000 runs reveals an 99.9% probability of failure, significantly higher than calculations neglecting strain-softening behaviour (Fig. 16b).

Fig. 17 shows the 3D failure volumes with the minimum FoS together with cross sections along the NL. The mobilised *Su* at the interslice levels (blue dots) and at the basal failure surface (red dots), shown in Fig. 17, demonstrate that sediment strength degradation occurs primarily at the base of the failure surface.

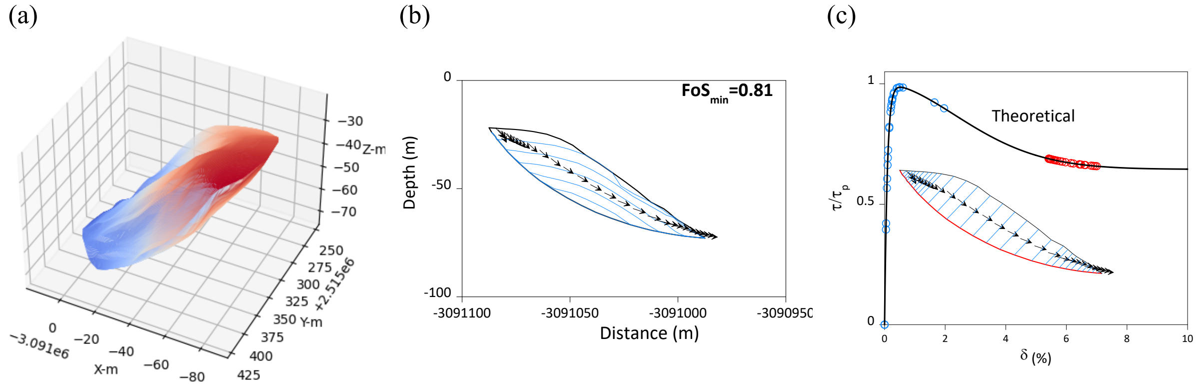

Fig. 17 For minimum FoS: **a** 3D failure surface and associated volume of 154,802 m^3, **b** 2D cross section along the NL of the slide, and **c** the mobilised Su at the interslice levels (blue dots) and at the base of the slide (red dots) demonstrating that sediment degradation occurs primarily at the base of the failure surface

Discussion

Complex morphology: 2D versus 3D analysis

Widely adopted for their simplicity, 2D slope-stability methods which simplify 3D morphology to 2D geometry, often affect the accuracy of the analysis. In general, the 2D approach tends to underestimate slope stability, and studies have consistently shown that 3D analysis produces higher factors of safety compared to its 2D equivalent (Albataineh 2006, Duncan 1996). 3D slope stability analysis is to a greater extent more efficient in the case of complex geometry, where the analysis results depend on the selection of a representative section for 2D analysis (Chakraborty and Goswami 2016). This is clearly demonstrated in the present analysis, where the FoS for a 2D cross section was nearly zero. It is obvious that for complex morphologies, such as that of the Nice slope, the 2D approach fails to provide values representative of slope stability, highlighting the need to solve the problem by including its 3D complex morphology and stratigraphy. Furthermore, it is clear that essential information and data, predominantly concerning volume and geometry crucial for landslide-tsunami analysis, can only be derived through comprehensive 3D analysis.

Limit equilibrium versus limit analysis

Results from the literature on 2D slope stability analysis have already shown that the limit equilibrium method tends to underestimate slope stability (Yu et al. 1998). Conversely, using the limit analysis method with an admissible kinematic velocity field provides an upper bound solution by minimising the work-energy balance equation. This approach helps to determine the external load (or FoS) leading to failure (Donald and Chen 1997). The disparity between these two methods is well demonstrated in Fig. 11, where the area characterised by a FoS of 0.6 with the limit equilibrium method corresponds to an average FoS value of 1.02 with the limit analysis method. However, it is crucial to acknowledge several differences between the two methods, including the shape of the failure surface (spherical for limit equilibrium and arbitrary for limit analysis), the neglected interaction between prisms in the limit equilibrium method, and differences in the theoretical approaches and the numerical optimisation methods. These factors may contribute to the observed differences in terms of FoS. Nevertheless, in this 3D analysis, despite the simplifications adopted in the limit equilibrium method, the results obtained are conservative and offer a clear indication of the most critical areas for further analysis using more advanced methods.

Deterministic versus probabilistic analysis

In the natural environment, the variability and heterogeneity of sediments are often inconsistent with the use of a deterministic approach (Christian et al. 1994), where each layer is characterised by a unique set of geotechnical properties. Analysis in undrained conditions, where the two essential parameters are *Su* and γ', our data clearly demonstrated the natural variability of the sediment, including a standard deviation of 3.1 kPa for *Su* and 0.75 kN/m^3 for γ' (Table 1). Despite this relatively low variability, the results clearly show the importance of incorporating this uncertainty into the analysis. A deterministic analysis using mean geotechnical values would lead to a FoS of 1.02 (Fig. 11) concluding the absence of a landslide by using a criterion that considers failure for FoS equal to or less than one. Conversely, the probabilistic analysis indicates a relatively high probability of failure (i.e. FoS $\leq$1) ranging between 18.3% and 19.9% (Fig. 14 and Fig. 15). These results highlight the advantage of analysing such a problem with a probabilistic approach, easily integrated in the framework of a PTHA analysis associated with the Tsunami-Landslide.

Perfectly plastic versus strain-softening material

The introduction in slope-stability calculation of the complex behaviour of natural sediment through strain softening appears crucial for sediments that may undergo degradation in mechanical properties, particularly shear strength during shearing (Conte et al. 2010, Troncone 2005). In the present study, we have demonstrated that a sensitivity of 1.55 significantly increases the probability of failure, shifting it from 19.9% (Fig. 15) to almost 100% (Fig. 16). It is worth noting that this concerns sediment characterised by a relatively low sensitivity of 1.55. These results emphasise the substantial error that a calculation considering a perfectly plastic sediment may involve. Our analyses also facilitate the precise determination of the location and geometry of the degraded zone (Fig. 7c) corresponding to the failure initiation zone. These output data can be considered as an input for models simulating the different phases of the development of a landslide event, ranging from initiation and growth to global failure and run-out (Zhang and Puzrin 2022). The introduction of strain softening, which represents the degradation of sediment during failure development, can also be associated with the concept of the destructuration index and the remaining energy available for runout, as suggested by Turmel and co-authors (Turmel et al. 2020). In conclusion, the introduction of strain softening, which often characterises the behaviour of natural clayey sediments, enables a more accurate determination of the probability of failure which appears significantly higher than in the case of an elastic plastic sediment. Furthermore, it provides essential elements for the analysis of post-failure processes, which are crucial aspects in the study of landslide tsunamis PTHA (Grezio et al. 2017).

Tsunamigenic efficiency calculation

Landslide-tsunami potential depends on multiple factors, including the efficiency of the landslide. In addition to landslide volume and mass discharge (Harbitz et al. 2006), this efficiency is directly linked to factors such as landslide geometry, coherence during the post-failure phase (mass fails as a single piece versus separated blocks), and water depth (Geist and Lynett 2014, Lynett and Liu 2002). A PTHA requires integrating the efficiency of the landslide, which is considered through a probability of occurrence and a probability of energy transfer to water with time. Generally, the probability is obtained through an analysis of the return period of an occurrence triggered by external phenomena such as earthquakes, sediment overloading, fluid activity, climate change, gas-hydrate decomposition, etc. Conversely, the probability associated with natural heterogeneity and sediment behaviour, including the degradation of mechanical properties, is frequently underestimated or neglected (Lacasse and Nadim 1998). Therefore, developing a deterministic approach to calculating FoS, wherein only a value ≤ 1 triggers a landslide appears simplistic in establishing a reliable and practical Landslide PTHA. For instance, Fig. 11 shows that the mean FoS value is 1.02, which is the value potentially obtained in a deterministic analysis, while the probability of failure exceeds 18%. We also demonstrated, for a simple case of gravitational instability, how the introduction of low sediment sensitivity (1.55) could strongly increase the probability of failure from 19.9% to almost 100% (Fig. 15 and Fig. 16). These notable uncertainties are mainly related to simplifying morphologies, disregarding the natural sediment heterogeneity, and neglecting the non-linear and softening behaviour of the sediment.

Conclusion

We investigated the impact of certain important approximations traditionally used in the analysis of submarine slopes and emphasized the consequences of such approximations on calculation results. Our conclusions can be summarised in the following four points:

- The presence of complex morphology is incompatible with 2D analyses. Selecting a typical 2D profile for slope analysis is highly challenging, making the obtained 2D results fundamentally invalid.
- Uncertainties related to the mechanical properties of sediment need to rely on a probabilistic approach, accounting for the natural variability of the sediment. Our specific analysis of the Nice slope highlights that relying solely on the average FoS fails to provide a comprehensive understanding of slope stability. Incorporating probabilistic analyses is therefore essential for an analysis involving landslide tsunami.
- Despite underestimating the FoS, the 3D approach using limit equilibrium (Scoops3D) provides a rapid insight into critical zones, facilitating the selection of areas for further analysis with advanced methods.
- Considering that the strain-softening behaviour of natural sediment has a major impact on calculation results, we have shown that neglecting this aspect in landslide analysis can lead to a significant underestimation of slope stability. Additionally, it is crucial to note that such analyses enable to identify the landslide nucleation zone and can therefore be coupled to models able to consider the different phases of a landslide ranging from growth and global failure to run-out. These aspects are essential in landslide-tsunami PTHA studies.

Funding

This work benefited from the support of the EU project EMSO (http://www.emso-eu.org/) and the MODAL project (ANR-17-CE01–0017) supported by Agence Nationale de la Recherche (ANR) and Deutsche Forschungsgemeinschaft (DFG, Grant KO 2108/26–1) in the framework of a French-German research program.

Acknowledgment

The authors are grateful to the captains and crews of the R/V L'Europe, R/V Atalante, R/V Pourquoi Pas? and R/V Marion Dufresne, for their assistance in acquiring bathymetry data, piston cores and piezocone data during the MD 124 / GEOSCIENCES 2 cruise (doi.org/10.17600/1200060), the PRISME cruise (doi.org/10.17600/7010090), the STEP 2015 cruise (doi.org/10.17600/15006100), the ESSPENF50 2015 cruise (doi.org/10.17600/15010900), the MaRoLiS PENFELD cruise (doi.org/10.17600/18000671) and the MaRoLiS 2021 cruise (doi.org/10.17600/18002394). Special thanks go to S. Murphy for fruitful discussions and useful comments.

Data availability

The bathymetry data acquired during the STEP 2015 cruise and presented in this study can be freely downloaded from https://sextant.ifremer.fr/Donnees/Catalogue#/metadata/21cf0621-0e0c-421e-b680-8191b90a318b.

Other data will be made available on reasonable request.

Declarations

Conflict of interest: The authors declare no conflict of interest.

References.

Albataineh N (2006) Slope stability analysis using 2d and 3d methods. PhD dissertation, University of Akron, University of Akron,

Andresen L and Jostad HP (2007) Numerical modeling of failure mechanisms in sensitive soft clay-application to offshore geohazards. In: OTC (ed) Offshore Technology Conference, OnePetro, Texas, USA,

Anthony EJ and Julian M (1997) The 1979 var delta landslide on the french riviera: A retrospective analysis. Journal of Coastal Research 13: 27-35.

Behrens J, Løvholt F, Jalayer F, Lorito S, Salgado-Gálvez MA, Sørensen M, Abadie S, Aguirre-Ayerbe I, Aniel-Quiroga I and Babeyko A (2021) Probabilistic tsunami hazard and risk analysis: A review of research gaps. Frontiers in Earth Science 9: 628772.

Bishop AW (1955) The use of the slip circle in the stability analysis of slopes. Geotechnique 5: 7-17.

Box GEP and Muller ME (1958) A note on the generation of random normal deviates. The annals of mathematical statistics 29: 610-611.

Bullard GK, Mulligan RP, Carreira A and Take WA (2019) Experimental analysis of tsunamis generated by the impact of landslides with high mobility. Coastal Engineering 152: 103538.

Bullard GK, Mulligan RP and Take WA (2023) Landslide tsunamis: Exploring momentum transfer to waves generated by a range of materials with different mobility impacting water. Landslides 20: 2619-2633.

Chakraborty A and Goswami D (2016) State of the art: Three dimensional (3d) slope-stability analysis. International Journal of Geotechnical Engineering 10: 493-498.

Chen ZY, Wang XG, Haberfield C, Yin JH and Wang YJ (2001) A three-dimensional slope stability analysis method using the upper bound theorem - part i: Theory and methods. International Journal of Rock Mechanics and Mining Sciences 38: 369-378.

Christian JT, Ladd CC and Baecher GB (1994) Reliability applied to slope stability analysis. Journal of Geotechnical Engineering 120: 2180-2207.

Conte E, Silvestri F and Troncone A (2010) Stability analysis of slopes in soils with strain-softening behaviour. Computers and Geotechnics 37: 710-722.

Dan G, Sultan N and Savoye B (2007) The 1979 nice harbour catastrophe revisited: Trigger mechanism inferred from geotechnical measurements and numerical modelling. Marine Geology 245: 40-64. doi: 10.1016/j.margeo.2007.06.011

Demers D, Leroueil S and d'Astous J (1999) Investigation of a landslide in maskinonge, quebec. Canadian Geotechnical Journal 36: 1001-1014.

Dey R, Hawlader B, Phillips R and Soga K (2015) Large deformation finite-element modelling of progressive failure leading to spread in sensitive clay slopes. Géotechnique 65: 657-668.

Dey R, Hawlader BC, Phillips R and Soga K (2016) Numerical modelling of submarine landslides with sensitive clay layers. Géotechnique 66: 454-468.

Donald IB and Chen Z (1997) Slope stability analysis by the upper bound approach: Fundamentals and methods. Canadian Geotechnical Journal 34: 853-862.

Duncan JM (1996) State of the art: Limit equilibrium and finite-element analysis of slopes. Journal of Geotechnical engineering 122: 577-596.

Fellenius W (1936) Calculation of the stability of earth dams. Congress Large dams, Washington, DC, pp 445-463

Garziglia S, Sultan N, Thomas Y, Ker S, Marsset B, Bompais X, Woerther P, Witt C, Kopf A and Apprioual R (2021) Assessing spatio-temporal variability of free gas in surficial cohesive sediments using tidal pressure fluctuations. Journal of Geophysical Research: Earth Surface 126: e2021JF006131.

Geist EL and Lynett PJ (2014) Source processes for the probabilistic assessment of tsunami hazards. Oceanography 27: 86-93.

Grezio A, Babeyko A, Baptista MA, Behrens J, Costa A, Davies G, Geist EL, Glimsdal S, González FI and Griffin J (2017) Probabilistic tsunami hazard analysis: Multiple sources and global applications. Reviews of Geophysics 55: 1158-1198.

Harbitz CB, Løvholt F and Bungum H (2014) Submarine landslide tsunamis: How extreme and how likely? Natural Hazards 72: 1341-1374.

Harbitz CB, Løvholt F, Pedersen G and Masson DG (2006) Mechanisms of tsunami generation by submarine landslides: A short review. Norwegian Journal of Geology/Norsk Geologisk Forening 86.

Hicks MA and Samy K (2002) Influence of heterogeneity on undrained clay slope stability. Quarterly Journal of Engineering Geology and Hydrogeology 35: 41-49.

Hungr O, Salgado FM and Byrne PM (1989) Evaluation of a 3-dimensional method of slope stability analysis. Canadian Geotechnical Journal 26: 679-686.

Islam N, Hawlader B, Wang C and Soga K (2019) Large-deformation finite-element modelling of earthquake-induced landslides considering strain-softening behaviour of sensitive clay. Canadian Geotechnical Journal 56: 1003-1018.

Juang CH, Zhang J, Shen M and Hu J (2019) Probabilistic methods for unified treatment of geotechnical and geological uncertainties in a geotechnical analysis. Engineering geology 249: 148-161.

Kelner M, Migeon S, Tric E, Couboulex F, Dano A, Lebourg T and Taboada A (2016) Frequency and triggering of small-scale submarine landslides on decadal timescales: Analysis of 4d bathymetric data from the continental slope offshore nice (france). Marine Geology 379: 281-297. doi: 10.1016/j.margeo.2016.06.009

Kopf AJ, Stegmann S, Garziglia S, Henry P, Dennielou B, Haas S and Weber K-C (2016) Soft sediment deformation in the shallow submarine slope off nice (france) as a result of a variably charged pliocene aquifer and mass wasting processes. Sedimentary Geology 344: 290-309. doi: 10.1016/j.sedgeo.2016.05.014

Krabbenhoft K, Lyamin A and Krabbenhoft J (2015) Optum computational engineering (optumg2). Computer software] Retrieved from https://www optumce com.

Lacasse S and Nadim F (1998) Risk and reliability in geotechnical engineering. Fourth International Conference on Case Histories in Geotechnical Engineering, University of Missouri--Rolla, St Louis, Missouri, pp 1172-1192

Leynaud D and Sultan N (2010) 3-d slope stability analysis: A probability approach applied to the nice slope (se france). Marine Geology 269: 89-106. doi: 10.1016/j.margeo.2009.12.002

Lo KY and Lee CF (1973) Stress analysis and slope stability in strain-softening materials. Geotechnique 23: 1-11.

Locat J and Lee HJ (2002) Submarine landslides: Advances and challenges. Canadian Geotechnical Journal 39: 193-212. doi: 10.1139/t01-089

Lunne T and Long M (2006) Review of long seabed samplers and criteria for new sampler design. Marine Geology 226: 145-165.

Lunne T, Powell JJM and Robertson PK (2002) Cone penetration testing in geotechnical practice. CRC Press,

Lynett P and Liu PLF (2002) A numerical study of submarine–landslide–generated waves and run–up. Proceedings of the Royal Society of London Series A: Mathematical, Physical and Engineering Sciences 458: 2885-2910.

Løvholt F, Glimsdal S and Harbitz CB (2020) On the landslide tsunami uncertainty and hazard. Landslides 17: 2301-2315.

Mahmoud M, Woeller D and Robertson PK (2000) Detection of shear zones in a natural clay slope using the cone penetration test and continuous dynamic sampling. Canadian Geotechnical Journal 37: 652-661.

Masson DG, Harbitz CB, Wynn RB, Pedersen G and Løvholt F (2006) Submarine landslides: Processes, triggers and hazard prediction. Philosophical Transactions of the Royal Society A: Mathematical, Physical and Engineering Sciences 364: 2009-2039.

Michalowski RL (1995) Slope stability analysis: A kinematical approach. Geotechnique 45: 283-293.

Mountjoy J and Micallef A (2018) Submarine landslides. Submarine geomorphology: 235-250.

Piper DJW, Shor AN and Hughes Clarke JE (1988) The 1929 "grand banks" earthquake, slump, and turbidity current. In: Clifton HE (ed) Sedimentologic consequences of convulsive geologic events, Geological Society of America, pp 0

Reid ME, Christian SB, Brien DL and Henderson S (2015) Scoops3d—software to analyze three-dimensional slope stability throughout a digital landscape. US Geological Survey Techniques and Methods, book 14.

Sassa K, Dang K, Yanagisawa H and He B (2016) A new landslide-induced tsunami simulation model and its application to the 1792 unzen-mayuyama landslide-and-tsunami disaster. Landslides 13: 1405-1419.

Satake K and Kanamori H (1991) Abnormal tsunamis caused by the june 13, 1984, torishima, japan, earthquake. Journal of Geophysical Research: Solid Earth 96: 19933-19939.

Skempton AW (1964) Long-term stability of clay slopes. Geotechnique 14: 77-102.

Sultan N, Garziglia S and Colliat J-L (2011) Gas hydrate occurrences and seafloor deformation: Investigation of strain-softening of gas-hydrate bearing sediments and its consequence in terms of submarine slope instabilities. In: OTC (ed) OTC, Houston,

Sultan N, Gaudin M, Berne S, Canals M, Urgeles R and Lafuerza S (2007) Analysis of slope failures in submarine canyon heads: An example from the gulf of lions. Journal of Geophysical Research-Earth Surface 112. doi: 10.1029/2005JF000408

Sultan N, Savoye B, Jouet G, Leynaud D, Cochonat P, Henry P, Stegmann S and Kopf A (2010) Investigation of a possible submarine landslide at the var delta front (nice continental slope, southeast france). Canadian Geotechnical Journal 47: 486-496. doi: 10.1139/t09-105

Synolakis CE, Bardet J-P, Borrero JC, Davies HL, Okal EA, Silver EA, Sweet S and Tappin DR (2002) The slump origin of the 1998 papua new guinea tsunami. Proceedings of the Royal Society of London Series A: Mathematical, Physical and Engineering Sciences 458: 763-789.

Tappin DR, Watts P and Grilli ST (2008) The papua new guinea tsunami of 17 july 1998: Anatomy of a catastrophic event. Natural Hazards and Earth System Sciences 8: 243-266.

ten Brink US, Chaytor JD, Geist EL, Brothers DS and Andrews BD (2014) Assessment of tsunami hazard to the us atlantic margin. Marine Geology 353: 31-54.

Tran TV, Alvioli M, Lee G and An HU (2018) Three-dimensional, time-dependent modeling of rainfall-induced landslides over a digital landscape: A case study. Landslides 15: 1071-1084.

Troncone A (2005) Numerical analysis of a landslide in soils with strain-softening behaviour. Geotechnique 55: 585-596.

Turmel D, Locat P, Locat J, Locat A and Leroueil S (2020) The energy reduction factor (f er) to model sensitive clay flowslides using in situ geotechnical and rheological data. Landslides 17: 839-853.

Urgeles R and Camerlenghi A (2013) Submarine landslides of the mediterranean sea: Trigger mechanisms, dynamics, and frequency-magnitude distribution. Journal of Geophysical Research: Earth Surface 118: 2600-2618.

Urlaub M, Talling PJ and Masson DG (2013) Timing and frequency of large submarine landslides: Implications for understanding triggers and future geohazard. Quaternary Science Reviews 72: 63-82.

Vanneste M, Forsberg CF, Glimsdal S, Harbitz CB, Issler D, Kvalstad TJ, Løvholt F and Nadim F (2013) Submarine landslides and their consequences: What do we know, what can we do? Landslide Science and Practice: Volume 5: Complex Environment: 5-17.

Yu HS, Salgado R, Sloan SW and Kim JM (1998) Limit analysis versus limit equilibrium for slope stability. Journal of Geotechnical and Geoenvironmental Engineering 124: 1-11.

Zengaffinen-Morris T, Urgeles R and Løvholt F (2022) On the inference of tsunami uncertainties from landslide run-out observations. Journal of Geophysical Research: Oceans 127: e2021JC018033.

Zhang G and Zhang JM (2007) Simplified method of stability evaluation for strain-softening slopes. Mechanics Research Communications 34: 444-450. doi: 10.1016/j.mechrescom.2007.06.001

Zhang W and Puzrin AM (2022) How small slip surfaces evolve into large submarine landslides—insight from 3d numerical modeling. Journal of Geophysical Research: Earth Surface 127: e2022JF006640.

Zhang W, Randolph MF, Puzrin AM and Wang D (2019) Transition from shear band propagation to global slab failure in submarine landslides. Canadian Geotechnical Journal 56: 554-569.